Frontiers of Aerothermodynamics

Chul Park
Department of Aerospace Engineering, Korea Advanced Institute of Science and Technology
Daejeon, Korea

Summary

Desirable directions of future research in the field of aerothermodynamics are described. The possible future human endeavors in high speed flight and likely problems needing to be solved therein are enumerated. This includes flights in Earth's atmosphere, entry flights into outer planets, and radiation and ablation phenomena. Recommendations are made as to how these problems could be approached.

1. Problems Involving Air Chemistry

1.1. Possible Future High Speed Flights in Earth's Atmosphere

1.1.1. Airbreathing Hypersonic Flight

Supersonic combustion is known to be limited by the rate by which air and propellant mix. When the Mach number at the inlet of a combustor reaches 1.5, the combustion efficiency is already substantially lower than unity, i.e. typically about 80%. At an inlet Mach number of 2, efficiency falls to about 50%. Operating at an inlet Mach number of 1.75, say, one can expect to operate a cruising vehicle at a flight Mach number of about 6 with hydrogen and about 4.5 with a hydrocarbon fuel. If an airplane is built using such an engine, its range is not sufficient to cross the Pacific Ocean or fly from London to Sydney. This means that probably there are no markets in the traditional commercial aviation for such an airplane.

Combustion is possible with a dimishingly small efficiency at higher Mach numbers. A positive thrust may be obtained to a Mach number as high as 12. But, if such a vehicle is used as an accelerator, i.e. to accelerate a payload to the orbital velocity, or to a sub-orbital but still interesting speed, its fuel economy is not demonstrated to be better than that for rocket propulsion. Therefore, markets for such a vehicle is unlikely.

One may ask whether a hypersoic vehicle has merit over a rocket-propelled vehicle in military applications. An airbreathing airplane has one advantage over a rocket-propelled vehicle in that it can easily evade an enemy interception: it can utilize its lift to change the flight path. For this reason, probably airobreathing hypersonic vehicle may be pursued for military purposes. In the present lecture, airbreathing hypersonic propulsion will not be considered.

1.1.2. Ballistic Flight

One emerging market for hypersonic technology is space tourism. A rocket-powered sub-orbital space vehicle may take passengers to an altitude above 100 km and let them experience a weightlessness for up to about 30 minutes. During the ascent and descent, such a vehicle produces an acceleration of about 3g's. To about 30 minutes, healthy persons are said to be able to withstand weightlessness, and endure such a g. One should be able to fly from London to Sydney, or from Seoul to Los Angeles, in such a vehicle for a fare of about 20,000 Euros. The existing first class fare for the same flight is of the order of 7000 Euros. Many predict that there will be enough customers to operate such a hypersonic service.

Such space tourism is a luxury and a leisure activity. Government organizations are not in the position to pursue its realization, because to do so would favor only the rich. The effort to realize space tourism will remain strictly in private sectors. But, within the private sectors, the effort will clearly be there.

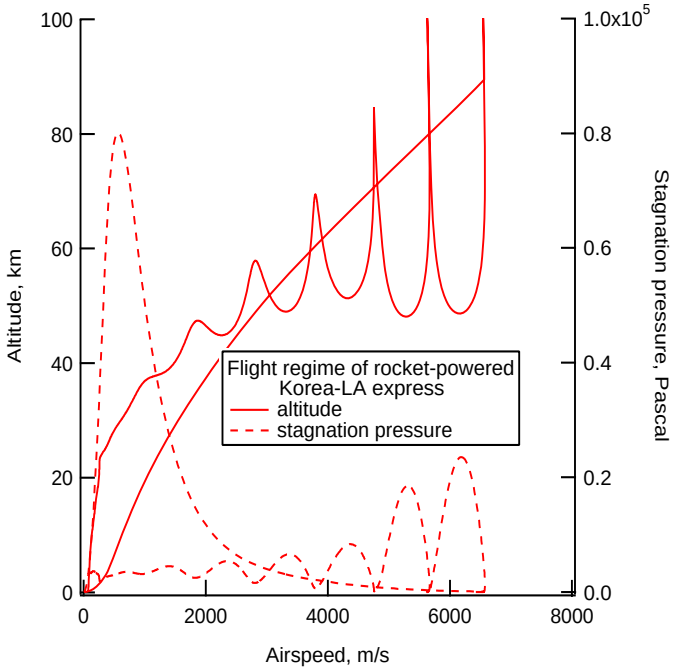

Figure 1. Flight regime of a ballistic airliner flying from Seoul to Los Angeles.

The maximum reentry Mach number of such a vehicle varies from about 5 to about 20 depending on the distance it flies. If the vehicle's flight Mach number is less than 5, the vehicle does not spend enough time above 100 km altitude to call it a space vehicle. In Fig. 1, the flight regime of a Seoul-to-Los Angeles ballistic airliner is shown. The figure shows that the vehicle's flight speed reaches 6 km/s. But the peak stagnation pressure in hypersonic speed range remains under 0.2 atm. Pressure must be kept so low in order to keep the acceleration below 3 g. At Mach 5, vibrational excitation will occur. At about Mach 7, dissociation of oxygen starts. At 6 km/s, even nitrogen may dissociate. Because of

low pressure, the flow around the vehicle will be dominated by nonequilibrium phenomena.

1.1.3. Lunar Missions

The current rush to the Moon can be said to have been motivated by China's declaration that it wants to send humans to the Moon. China's reason to go to the Moon is said to be "to resume the quest of Admiral Zheng He which was stopped abruptly in the year 1421". In 1421, China stopped the exploration of the world with some two hundred ships. Those ships sailed to the tip of Africa, or maybe even to the American continent. An emperor's edict in 1421 stopped it for the reason that there was no justification for continuing the quest. As a result, China went to sleep for the following five centuries in science and technology. China is vowing that it will never repeat that mistake. This time, Chinese will not ask why they go to the Moon or Mars, so that there will be no reason to stop it either.

There are said to be two goals of going to the moon: finding water and finding helium-3. If we find water, we can live there. Using solar or nuclear energy, water can be split into hydrogen and oxygen, which can power rocket ships. Helium-3, an isotope of helium with a molcular weight of 3, is an ingredient needed for thermonuclear fusion. It is needed only in a small quantity. At least theoretically, an operating fusion reactor both consumes and produces helium-3 simultaneously. By desining the operating condition appropriately, more helium-3 can be made than used. That is, breeding is possible. But, before such a breeder fusion reactor is made, helium-3 will be needed. Also, even when breeder reactor is completed, it is needed in oder to start the reactor, in the role of a primer.

In order to bring back helium-3, earth reentry must be executed. In order to repeat this activity, both the launch vehicle and reentry vehicle should preferably be reusable. The recovery of the first and possibly the second stage rocket vehicles will require precesion in aerothermodynamic prediction capability. The technology of reentry developed for Apollo entry must be improved to meet this requirement.

1.1.4. Orbital Balloons

A few years ago (circa 2002), Lockheed-Martin and Boeing separately and independently examined the feasibility of building a fully reusable two-stage-to-orbit launch system. Both companies failed to design a viable such system. The reason was that the requirement that the reusable first stage returns to the launch point could not be satisfied. The first stage attains a flight Mach number of four or more at the time of staging. At such a high speed, 180-degree U-turn is impossible without losing altitude drastically. To return to the launch point, the first stage vehicle has to slow down to a subsonic speed, make a U-turn, and fly back using conventional jet engines. But the vehicle has a lift-to-drag ratio of no more than 3. For such a vehicle to fly back nearly 1000 km, powerful engines and

a large amount of fuel are needed. These engines produce such a large frontal area that acceleration to a hypersonic speed becomes impossible.

Solution to this problem is obvious: remove the requirement to return to the launch point. If, for instance, the launch is made in California, the first stage can land in New Mexico or Texas. The vehicle can refuel and fly back to the launch point the next day. This option was not pursued because a government cannot expose its citizens to a possible danger of a spacecraft crashing on them. But a private company could do this by paying an insurance company.

Another possibility is to use international cooperation. One could make the launch at the eastern shore of Vietnam, and recover the first stage in The Phillippines, or make a launch at an east coast of Africa and recover the first stage in India, etc. There are many such combinations on the globe. These are not pursued because the space program involves national security. If the space activity becomes a purely commercial enterprise, such international cooperation will happen.

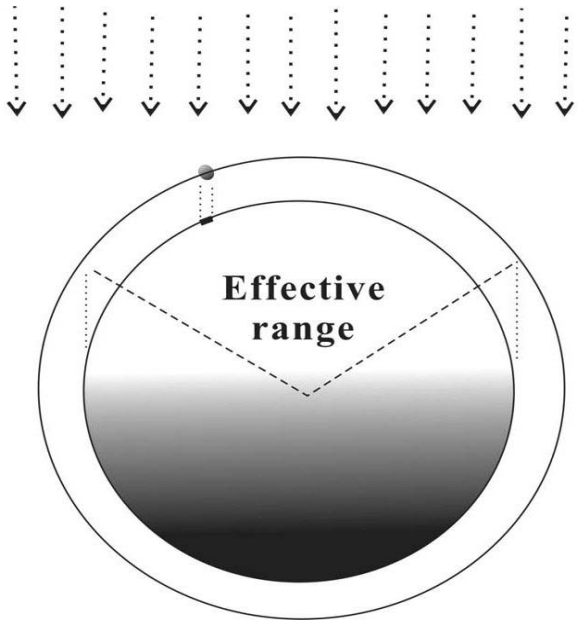

Figure 2. Orbital balloons blocking sun[1].

In Ref. 1, a proposal was made to cool the Earth and thereby solve the global warming problem by letting many large balloons circle the Earth in orbits, as shown schematically in Fig. 2. Each balloon is made of a thin plastic sheet, has a diameter of the order of 50 km, and a mass of the order of 10,000 tons. One or two hundreds of these balloons in altitudes of 1000 to 2000 km will cool the Earth sufficiently. To do so, one or two million tons of material must be placed in orbits every 30 years or so. The cost of this endeaver will be charged to the CO_2 producers proportionately to its amount they produce. The activity of placing the balloons will go to the multinational private companies through a

competitive bidding process.

This is truly a star war scenario, except that the enemy is global warming. Though costly, this is probably the only assured way of combating global warming. If human race accepts this solution, there will be a serious need to develop a reusable launch system.

1.2. What More Do We Need in Aerothermodynamics in Air?

1.2.1. Shock Stand-off Distance

In the past decade or so, efforts have been made to tune methods of calculating nonequilibrium flows in air to agree with experimental data taken in a shock tunnel. Flow Mach numbers based on enthalpy were from about 10 to about 15, which may be called 'intermediate hypersonic' regime. The separated flow over a double cone was chosen for this purpose (see, e.g., Ref. 2). After several years of effort, we now see a fairly good agreement. The so-called two-temperature model was used in these calculations.

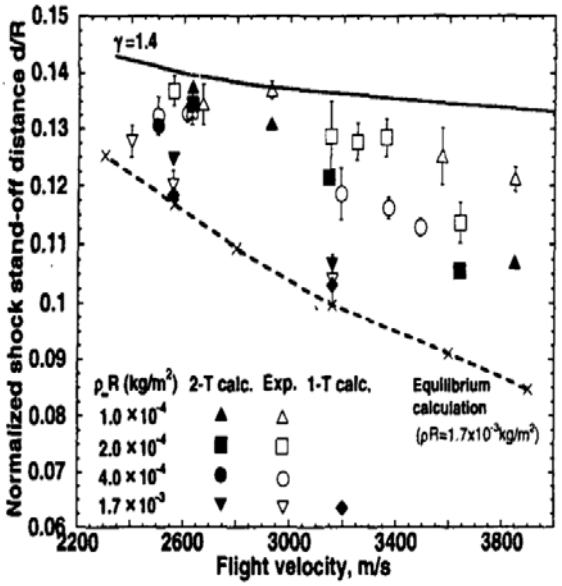

Figure 3. Comparison of shock stand-off distance over a sphere between ballistic range test and computation[2]

However, there is still a small question left. In Fig. 3, comparison is made of the shock stand-off distance over a sphere between ballistic range experiments[3] and computation[4]. As seen in this figure, calculation slightly underestimates the shock stand-off distance at Mach number of about 10 and 12. This is surprising. In any experiment, there is impurity in the flow. This impurity tends to make the effective gamma smaller than assumed. This tends to make the shock stand-off distance smaller in experiment. That is, calculation always overestimates shock stand-off distance. Furudate and Sawada[4] concluded that this discrepancy can be explained only by assuming that rotational relaxation is slow.

In the existing two-temperature model, rotationalal mode is assumed to be in equilibrium with translational mode, that is, rotational relaxation is infinitely fast. That rotational relaxation is slow has serious implifications. If the shock stand-off distance is not calculated correctly, shock shape is not calculated correctly. If shock shape is not calculated correctly, pressure distribution and hence lift, drag, and moments are not calculated correctly. This discrepancy probably makes only a small error in lift and drag coefficients. As with any other technology, aerothermodynamics is in the position to having to remove last small errors. This problem is one frontier left for aerothermodynamics.

1.2.2. Experimental Evidence of Rotational Nonequilibrium

Rotational temperature can be measured relatively simply by analyzing the spectrum of radiation from a hot gas. One produces a strong shock wave in a shock tube, and observes radiation behind it. In air or in nitrogen, N_2 First and Second Positive bands, N_2^+ First Negative bands, and NO γ band occur prominentaly. To analyze the spectrum observed, one needs a computer code. The code NEQAIR85[5] has been distributed freely throughout the world, which can be used for this purpose. The code spawned many similar codes. The measured rotational temperature can then be compared with the calculated translational temperature to see whether the assumption that the two temperatures are equal is valid.

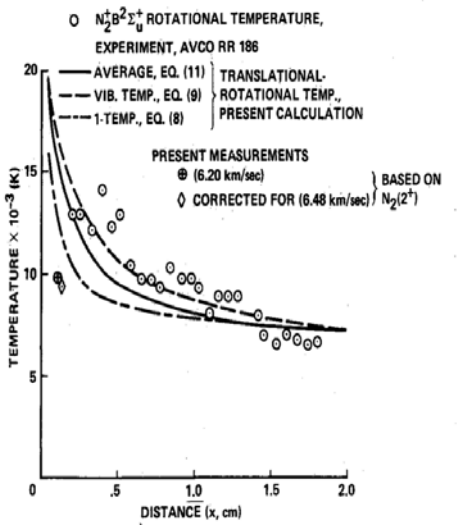

Figure 4. Comparison between the measured rotational temperature and calculated translational temperature; measurement by Sharma[6].

Fig. 4 shows the measurement by Sharma et al.[6] The data clearly shows that the rotational temperature is smaller than the calculated translational temperature. In Fig. 5, similar comparison is made for the measurement by Fujita et al.[7] In Fig. 6, similar comparison is made for the measurement by Koreeda[8]. In Fig. 7. similar comparison

is made for the measurement by Miyazaki et al[9]. The data by Miyazaki et al deserves particular attention: unlike the three other data, which measured rotational temperature of an electronically excited state of N_2 molecule, this data were taken with the ground electronic state. Thus, there is little doubt that rotational temperature does not follow translational temperature behind a strong shock wave.

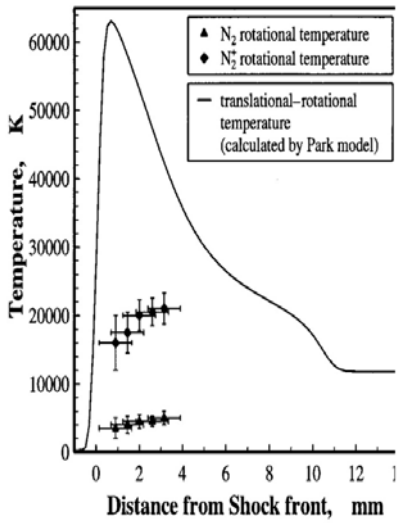

Figure 5. Comparison between the measured rotational temperature and calculated translational temperature; measurement by Fujita[7].

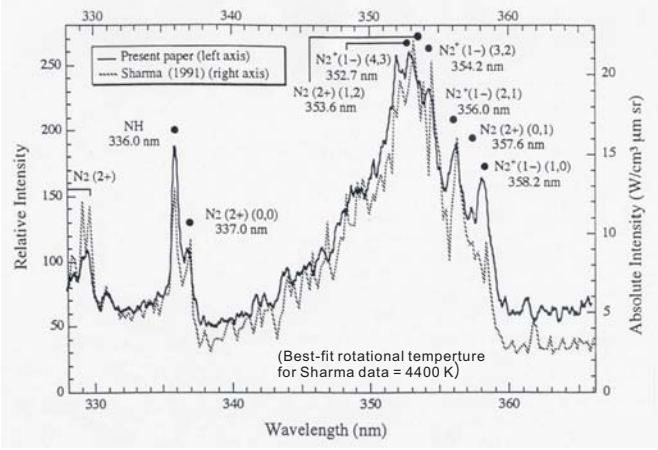

Figure 6. Comparison between the measured rotational temperature and calculated translational temperature; measurement by Koreeda[8].

1.2.3. Theoretical Effort on Rotational Relaxation

In order to explain the experimental data showing rotational nonequilibrium, an effort was made to theoretically calculate the rotational relaxation phenomenon. Park[10] calculated the rotational relaxation phenomenon in N_2. There is a set of experimental data giving the rotational state-to-state transition rates for N_2 for rotational levels of up to 15

(Ref. 10). He used and extended this data into higher rotational levels. His results are shown in Figs. 8 and 9. According to his results, at translational temperature above about 11,000 K, rotational relaxation rate becomes indistinguisable from vibrational relaxation rate.

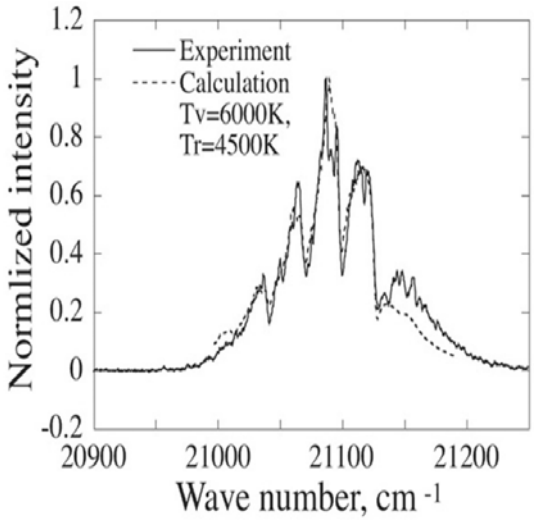

Figure 7. Comparison between the measured rotational temperature and calculated translational temperature; measurement by Miyazaki et al[9].

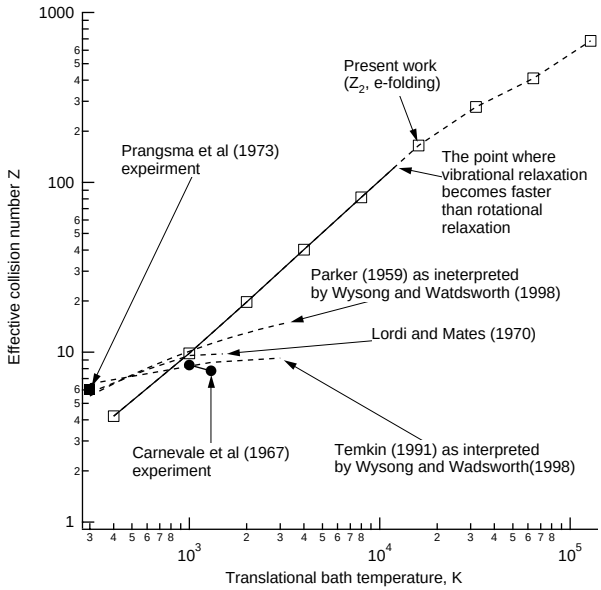

Figure 8. Collision numbers required for equilibration of rotational mode for N_2 calculatede by Park.[10]

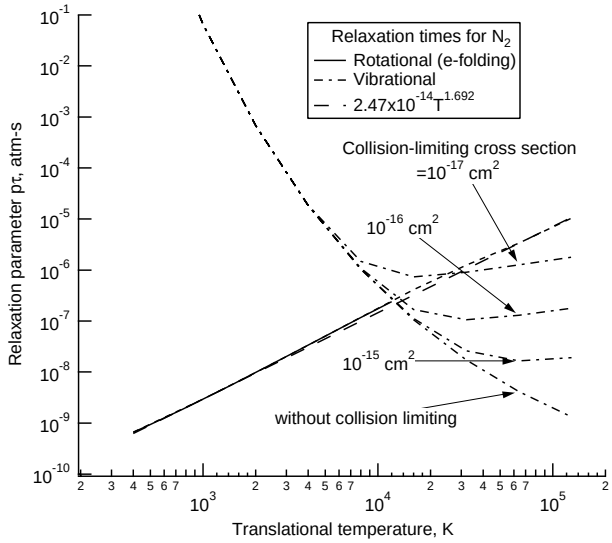

Figure 9. Rotational relaxation time for N_2 calculated by Park.[10]

Using Park's rotational relaxation model, the shock tube measurement by Fujita et al can be numerically reproduced reasonably closely, as seen in Fig. 10.

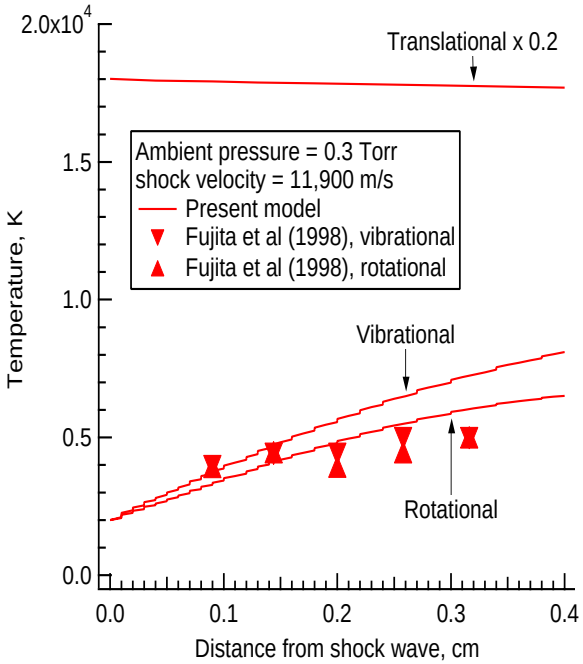

Figure 10. Comparison between the experimental data of Fujita[7] **and Park's rotational model.**[10]

Despite this success, Park's rotational relaxation model for N_2 cannot be considered

totally reliable because such a far extrapolation was used. A more complete model was sought for H_2. For H_2, potential energies during the collisions of H_2 + H and H_2 + H_2 are both known. By carrying out molecular dynamics calculations, one can determine the state-to-state collisional transition rate coefficients accurately. Using those state-to-state transition rates, master equation calculation can be made. From the master equation calculation, one can deduce the rotational relaxation rates and times. The state-to-state transition rate calculation has been carried out for H_2 + H first by Sharma and Schwenke[11]. Unfortunaely, they did not produce the rotational relaxation rates in a usable form.

Similar effort was made by Furudate et al.[12] They produced rotational relaxation time values. According to their calculation, rotational relaxation becomes faster at higher temperatures rather than slowing down. However, when their state-to-state rate data were used to compute the recombination rate H + H + H_2 → H_2 + H_2, the calculated recombination rate did not agree with the measured values. Only by dividing their state-to-state rates by $\sqrt{T/1000}$, did their calculation match experimental data.[12] In Fig. 11, this behavior is shown.

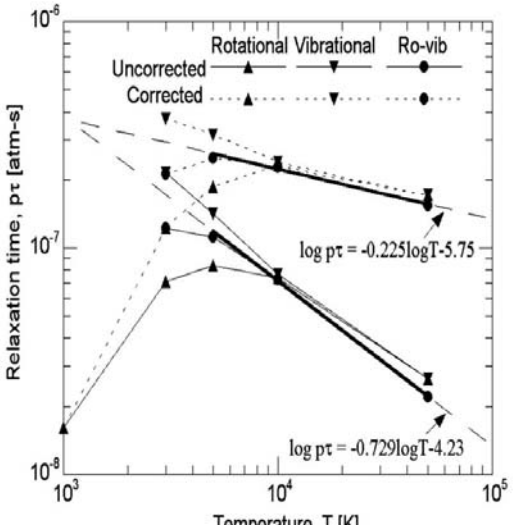

Figure 11. Comparison between the calculation of Furudate and Fujita and experiment on hydrogen recombination rates.[12]

A similar effort was made by Kim et al[13] for H_2 + H interactions. Their calculation led to a result totally opposite of that by Furudate et al. They showed that rotational relaxation occurs no faster than vibrational relaxation at high temperatures. In Fig. 12, their results are shown.

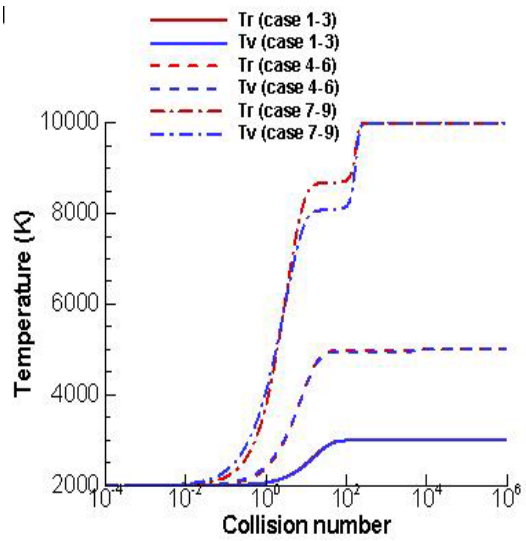

Figure 12. Relaxation of vibration and rotation in H_2 by collisions of H calculated by Kim et al.[13]

Thus, there are sufficiently large numbers of clues to believe that rotational relaxation at high temperature occurs at about the same rate as vibrational relaxation. This means that the existing two-temperature model is invalid at high temperatures. At high temperatures, rotational and vibrational modes could be considered coupled, leading to a new kind of two-temperature model. However, in the intermediate temperature range where the two modes are not quite coupled, a three-temperature description may be necessary. A new modeling is needed toward this end. To do so, the first step is to be able to compute the state-to-state transition rate coefficient for vibrational and rotational states. Then one must develop a technique of handling a large number of rate coefficients in integrating the master equation.

1.2.4. Other Shortcomings in Two-Temperature Model

The existing two-temperature model has several adjustable parameters. The first is the so-called collision-limiting cross sections in vibrational relaxation. This concept was introduced in order to correct the Millikan-White formula at high temperatures. Millikan-White formula on vibrational relaxation time predicts an unrealistically small relaxation time at high temperatures. The two-temperature model says that the relaxation time cannot be smaller than that dictated by elastic collisions. The limiting elastic collision cross sections had to be guessed. Even though the concept of collision-limiting is valid, there is no need to guess any more. The SSH theory, forced oscillator theory, and molecular dynamics calculation all are able to produce the effective elastic cross sections. In Figs.

13(a) to (c), the vibrational relaxation times calculated by the forced oscillator model are shown. In Fig. 14, the relaxation times calculated by the SSH theory are shown. These figures show the trend that the relaxation time deviates upward at high temperatures, i.e. the trend that collision-limiting theory describes.

In order to carry out what is described here, one must be able to handle the large set of state-to-state transition rates in a large master equation set. Total number of states will be in tens of thousands, and the number of state-to-state rate coefficients will be square of those. It is at this time not possible to carry out such a calculation. A new method has to be developed to enable such a master equation calculation. A very innovative idea is needed here.

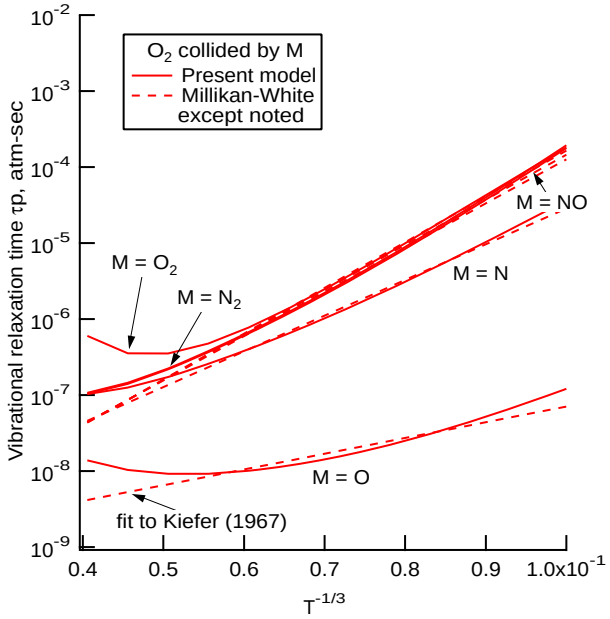

Figure 13. Vibrational relaxation time calculated by forced oscillator model. (a) O_2^{14}.

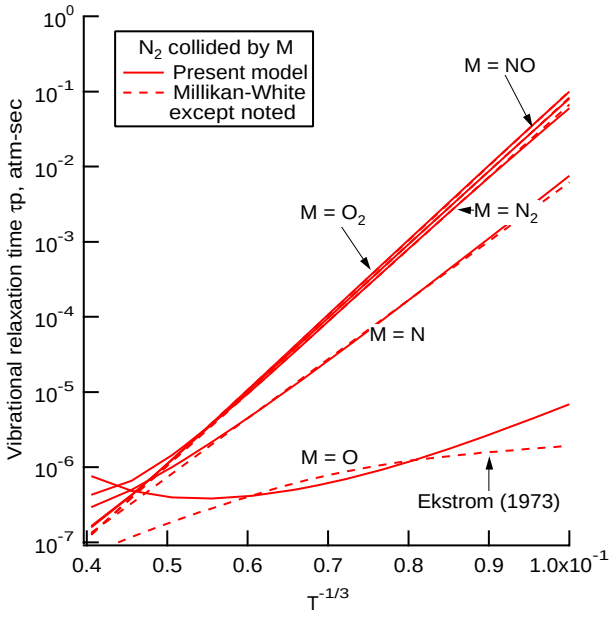

Figure 13. (b) N_2^{14}.

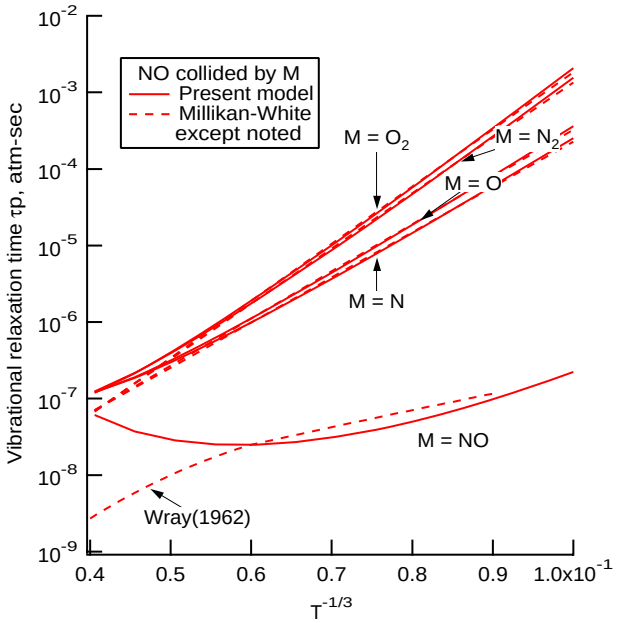

Figure 13. (c) NO^{14}.

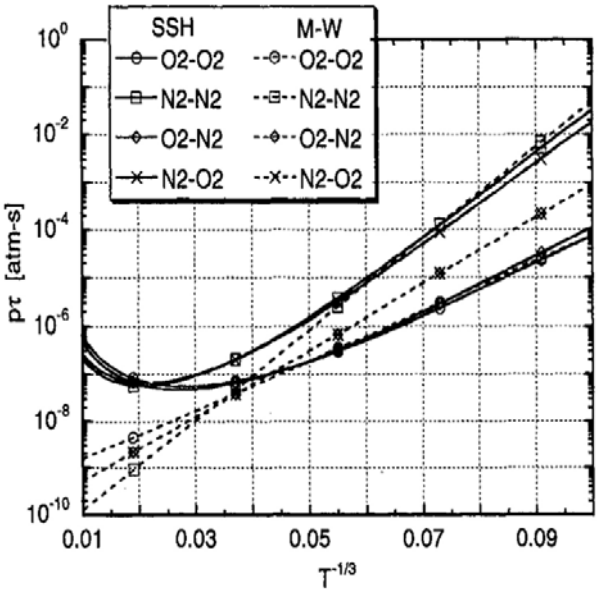

Figure 14. Vibrational relaxation times for N_2, O_2, and NO calculated by SSH theory.[14]

Next adjustable parameter is the so-called diffusion correction for the Landau-Teller equation represented by the parameter S which varies from 1 to 3.5. A detailed master equation calculation[14] shows the diffusion phenomenon. Instead of an ad hoc values of S in the existing two-temperature theory, a more precise value should be able to be derived through a master equation calculation. This remains to be done in the future.

Finally, there is a question as to whether the geometrically averaged temperature $T_{av} = \sqrt{TT_v}$ can be improved. The latest calculation by Kim et al[13] shows that this geometrically-averaged temperature is useful for H_2 even when rotational mode is in nonequilibrium. Thus, it is uncertain at this time as to how the three-temperature environment should be described. Everybody is invited to tackle this problem.

2. Entries To Outer Planets

2.1. Jupiter's Moons

Planetary entries are one of the most exciting human endeavors. We expect this activity to continue. Not only the U.S., Europe, and Japan, but also emerging Asian powers aspire also to carry out such missions. Europe carried out a mission to Titan. But that mission used propulsive deceleration part of the way, so that the entry speed was only about 5 km/s. If propulsive deceleration is not used, the entry speed would have been much higher. In the future, entry speed of up to about 12 km/s must be considered.

Entry flights to the moons of Jupiter are also quite attractive. The atmospheres of these satellites differ chemically. Radiation will be a major part of heating of the entry vehicles. The dimensions of such vehicles will be of the order of 1 m, as the Titan entry vehicle made by Europe was. Because of the relatively small size, the shock layer flows around such vehicles will be in thermochemical nonequilibrium state.

One expects that, some day, humans will send a probe into the four large moons of Jupiter, all of which have an atmosphere though thin. The SO_2 atmosphere of Io, H_2O atmosphere of Europa, O_2 atmosphere of Ganymede, and CO_2 atmosphere of Callisto all deserve human expedition. All these entries will accompany radiation under nonequilibrium condition. Shock tube study of radiation phenomena with these gases will have to be made. Shock speed of the order of 12 km/s will have to be produced in such a shock tube with these gases.

2.2. Outer Planet Entries

2.2.1. Entry Flowfields

The entry fight into planet Jupiter by the U.S. was very fruitful. A similar mission is desired for Saturn, Neptune, and Uranus. For the Jovian entry, stagnation pressure was about 5 atm at the peak-heating point. Temperature immediately behind the shock wave was over 40,000 K. Because of the high pressure and temperature, the shock layer flow was nearly in equilibrium at the peak-heating point. Entry flightes into Saturn, Uranus, and Neptune will occur at lower pressures and lower temperatures.

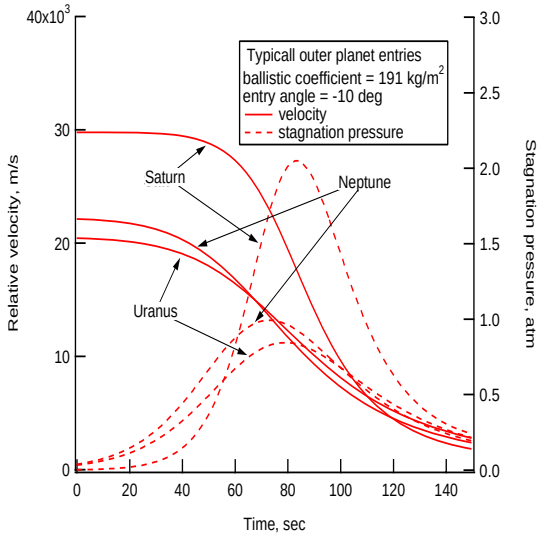

Figure 16. Velocity and stagnation pressure in typical entry flights into outer planets.

In Fig. 16, velocity and stagnation pressure are shown for a typical entry flight into Saturn, Uranus, and Nedptune. One sees in this figure that the peak stagnation pressure

is below about 2 atm. Depending on the thermochemical relaxation rates, the shock layer flow in these entry flights may or may not be in thermochemical equilibrium.

In Figs. 17(a) to (c), the nonequilibrium flow calculation is made behind a normal shock wave for the outer planet entries. The rate coefficients used in these calculation are taken from Furudate et al.[15] As these figures show, the flow is in a nonequilibrium condition at least part of the shock layer thickness. But the temperatures occurring in this case are far outside of the range of validity of those rate coefficients. Therefore, the accuracy of these figures is not at all assured.

However, if Figs.17(a) to (c) are to be believed at all, then one expects a radiation overshoot in the nonequilibrium region: strong radiation will occur where vibrational temperature is high. This occurs because ionization occurs while dissociation is still in progress. The atmospheres of these outer planets contain a small concentration of methane. Radiation of carbon atoms and CH will be interesting.

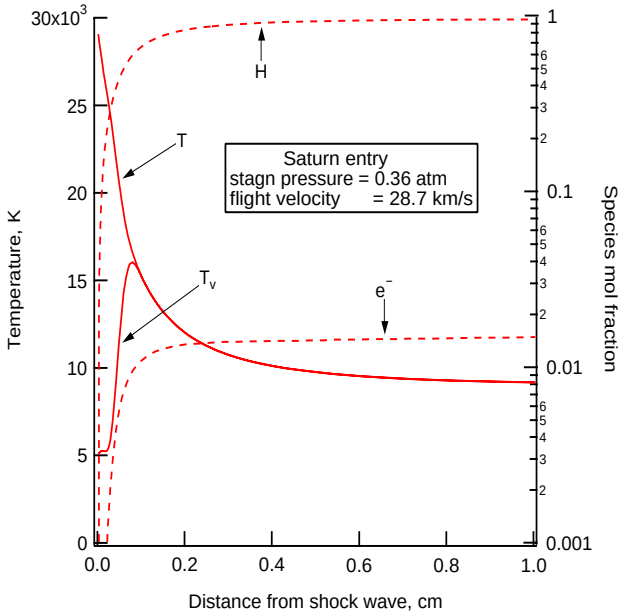

Figure 17. Anticipated flow environment behind a normal shock wave during an entry flight into outer planets. (a) Saturn.

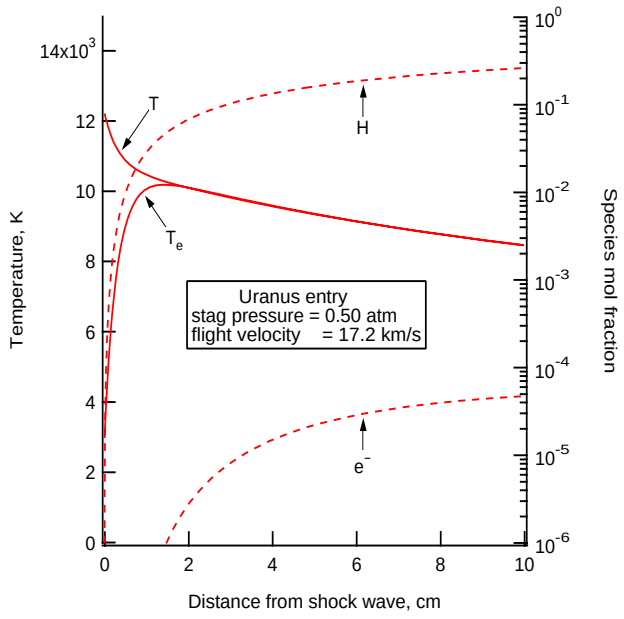

Figure 17. (b) Uranus.

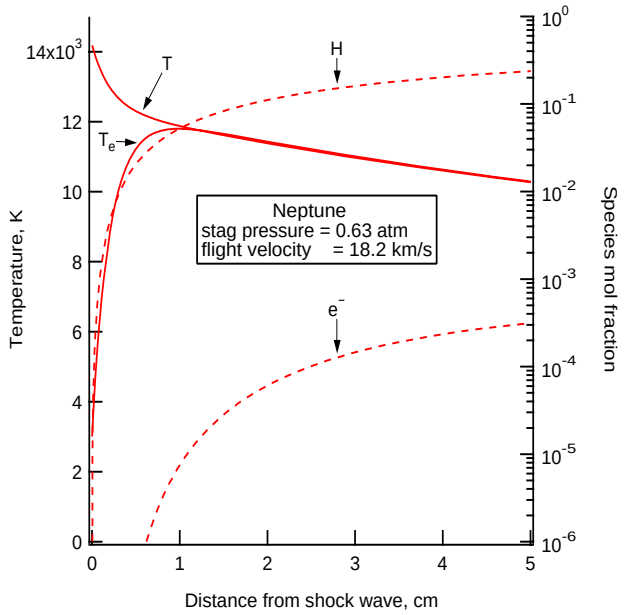

Figure 17. (c) Neptune.

2.2.2. Incipient Ionization

The electron density values shown in Figs. 17(a) to (c) were calculated using the model used by Furudate et al.[15]. However, accuracy of the model is at this time not assured. In the H_2 + He mixture, ionization must start with heavy particle impact ionization

$$H + H \rightarrow H^+ + e + e \quad (1)$$

or the associative ionization

$$H + H \rightarrow H_2^+ + e \quad (2)$$

Both these reactions in reality occur through a ladder-climbing process, the first step of which is

$$H(1) + H(1) \rightarrow H(2) + H(1) \quad (3)$$

where the numbers in the parentheses indicate principal quantum numbers. There are several theoretical research papers on the processes

$$H(1) + H(n) \rightarrow H_2^+ + e \quad (4)$$

The step (3) has the largest endothermicity and therefore is the rate-limiting step. Unfortunately, there are no theoretical papers on this most important process.

Leibowitz[16] carried out a shock tube experiment using an electric arc-driven shock tube to measure the ionization process of a H_2 + He mixture. He measured the rise in electron density behind a normal shock wave. From his experiment, he deduced what the rate of processes (1) and (2) should be. His values were used by Furudate et al[15] and in the present work in producing Figs.17(a) to (c).

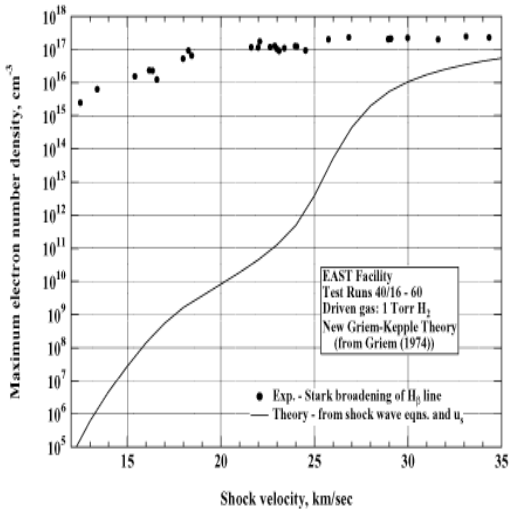

Figure 18. Comparison of electron density between measurement[17] in an electric arc shock tube and calculations.

Recently, Bogdanoff and Park[17] carried out an experiment in an electric arc-driven shock tube to reproduce the results of Leibowitz.[16] The experiment was a failure. They found that the flow upstream of the normal shock wave was ionized already by the irradiation from the luminous driver gas. The irradiation also heated the flow behind the normal shock wave intensely. As a result, the flow was ionized much more than it should. This result is shown in Fig. 18. This is a unique phenomenon occurring only when H_2 + He is used in an electric arc-driven shock tube. The flow velocity is so fast in this case that the arc discharge in the driver is not yet extinguised when the shock front reaches the test

section. Even though the shock tube used by Leibowitz was not the same as that used by Bogdanoff and Park, it was still an electric arc-driven shock tube. Therefore, the results of Leibowitz are in doubt.

In the H_2 + He flow under consideration, the excitation of the n = 2 state can occur radiatively through absorption of the Lymann α line irradiated from the downstream region.

$$H(1) + h\nu \rightarrow H(2) \tag{5}$$

If process (5) is dominant, process (3) becomes irrelevant. Park[18] made an effort to calculate the rate of process (1) under this environment. His result is shown in Fig. 19. In this case, the ionization rate becomes a function of the intensity of radiation. This is a radiation-controlled rate process. This is one area where further research is needed.

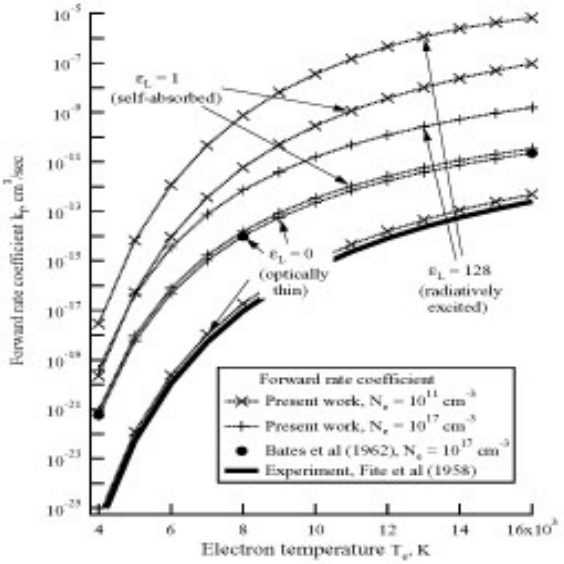

Figure 19. Ionization rate of H under irradiation of Lymann α radiation[18].

2.2.3. Needs for Shock Tubes

The above consideration leads one to conclude that more shock tube experiments are needed. The shock tube should be able to produce a shock speed of 12 km/s in air, N_2, or CO_2, SO_2, H_2O, and 30 km/s in H_2 + He mixtures. Up to now, electric arc-driven shock tube in NASA Ames Research Center was considered to be the answer. However, the findings by Bogdanoff and Park[17] leads one to look elsewhere. The only other alternative to electric arc driver is to use a piston compression-driven two-stage shock tube. The shock tube is identical to the so-called expansion tube[19]: it has three chambers, driver,

intermediate tube, and acceleration tube. But, unlike the expansion tube, the gas in the acceleration tube is used as the test gas. The setup is shown schematically in Fig. 20.

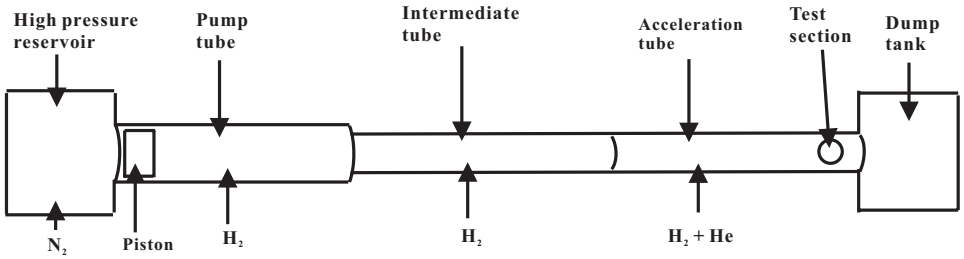

Figure 20. Schematic of piston compression-driven two-stage shock tube to produce 30 km/s in H_2+He mixture.

This is the type of the facilities used by Fujita et al[7], Koreeda[8], and Miyazaki et al[8]. Howeveer, their facilities seem to have been too small (internal diameter less than 50 mm). In order to obtain accurate data, diameter has to be larger. The facility in University of Queensland[19] is sufficiently large, but is not configured to use the gas in the acceleration tube.

3. Radiation and Ablation

3.1. Flight Data

3.1.1. Apollo[20]

The thickness of the heatshield for the Apollo Command Module was 55 mm. At the time, this thickness must have been thought of having a large safety margin. After the flight, when the heatshield was sectioned, 28 mm was seen to have undergone pyrolysis. That is, the heatshield was found to have been designed with a barely enough safety factor. Even though the entry flights of the Apollo vehicle were successful, one cannot be sure of what will happen if the heatshield material is changed. The uncertainty about the heating and ablating environment of the Apollo vehicles stems from the uncertainty about the extent and effect of radiation.

Prior to the flight of the moon missions, radiative heat flux was measured in a flight experiment called Apollo 4. At the peak heating point of its flight trajectory, the received radiation intensity was 25 W/(cm^2-sr) in the wavelength range from about 200 nm to about 4000 nm. Many researchers were able to numerically reproduce this value of radiation intensity.[20] In a most rudimentary way, by multiplying this intensity value by 2π, one obtains 158 W/cm^2 to be the radiative heat flux reaching the wall. The calculated Fay-and-Riddel convective heat transfer rate, ignoring the blowing effect of ablation, was 230 W/cm^2. Some of the two, 158 + 230 = 388 W/cm^2, is frequently said to be the heat flux received by the surface.

This 388 W/cm^2 of heat flux falls short of producing the observed extent of ablation. Moreover, the ablation phenomenon should have produced a significant reduction in the convective heat flux by the so-called convective blockage effect of blowing. The most thorough analysis of this problem was made by Park[20]. According to the analysis, at the peak-heating point of Apollo 4, the radiative flux at the edge of boundary layer was 394 W/cm^2, about of half of it being in the vacuum ultra-violet wavelength range. Because of the blowing, the convective heat flux in the absence of radiation should be 118 W/cm^2. But, absorption of radiation in the boundary layer increased convective heat flux to 363 W/cm^2. That is, there was a conversion of radiative heat flux into convective heat flux: out of 374 W/cm^2, 363 - 118 = 245 W/cm^2 was converted to convective heat flux. The remainder, 129 W/cm^2 was convected downstream.

That so much of radiative energy was absorbed in the boundary layer can be seen in the calculated spectrum at the peak heating point, shown in Fig. 21. The distribution of radiative heat flux in the shock layer is shown in Fig. 22.

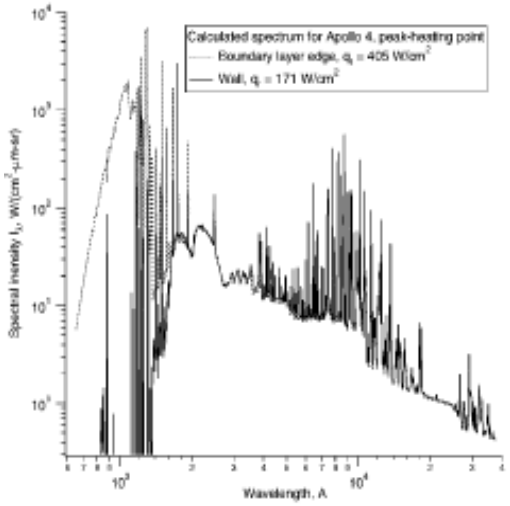

Figure 21. Calculated spectrum at the edge of boundary layer and at wall for Apollo 4 at the stagnation point.[20]

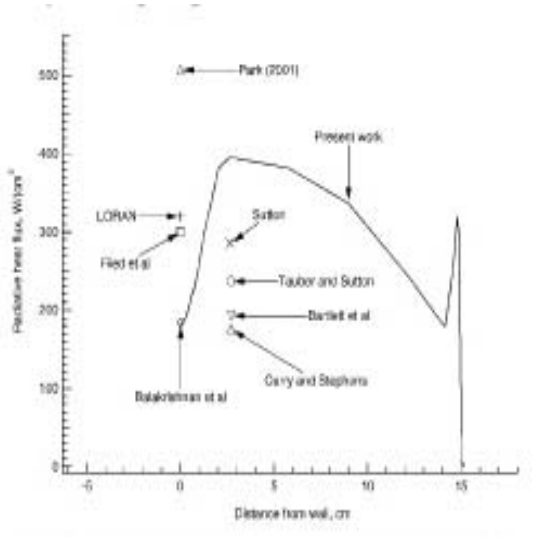

Figure 22. Calculated distribution of radiative heat flux along the stagnation streamline for Apollo4[20].

After the flight of Apollo 4 vehicle, the heatshield was sectioned. The density of the heatshield was measured at several locations. The result is plotted in Fig. 23.

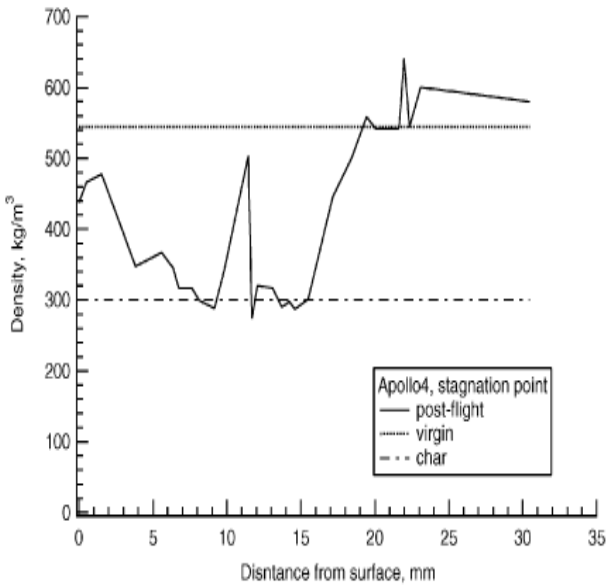

Figure 23. Density distribution in Apollo heatshield after flight.[20]

As the figure shows, the density in the char was higher than the theoretical density of the matrix. This is believed to be due to condensation of carbonaceous substances in the matrix, which is termed coking phenomenon. Because of the coking phenomenon,

the pyrolysis gas ejected from the wall probably contained little carbon. This will change the absorption phenomenon in the boundary layer. This phenomenon will occur even if heatshield material is changed. As yet, no study was made of this phenomenon. Someone will have to study this phenomenon in the future.

3.1.2. Galileo Probe

On the heatshield over the Galileo Probe vehicle that entered into the atmosphere of the planet Jupiter, there were sensors for the thickness of the heatshield. The sensors successfully transmitted the progress of surface recession during the entry flight. There have been several attemps to numerically recreate the measured recessions. The latest and most successful was the one by Matsuyama et al.[21] In Fig. 24, their calculation is compared with the flight data.

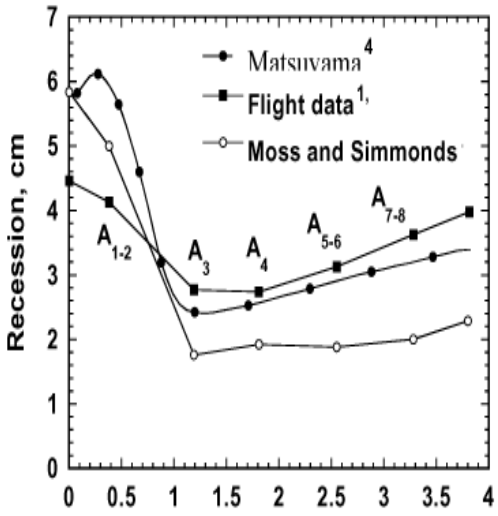

Figure 24. Comparison between the flight data and calculations onheatshield for Galileo Probe.[21]

As seen here, the latest calculation agrees with the flight data on the downstream portion of the heatshield. In the stagnation region, however, the calculation over-predicts. Recently, Park[22] calculated the stagnation region heating environment for Galileo Probe using an accurate method of calculating the equilibrium composition, accounting for more radiation absorption mechanism in the boundary layer, and radiation blockage by the solid particles ejected from the heatshield surface. His calculation is compared with the flight data in Fig. 25. As seen in the figure, agreement is good.

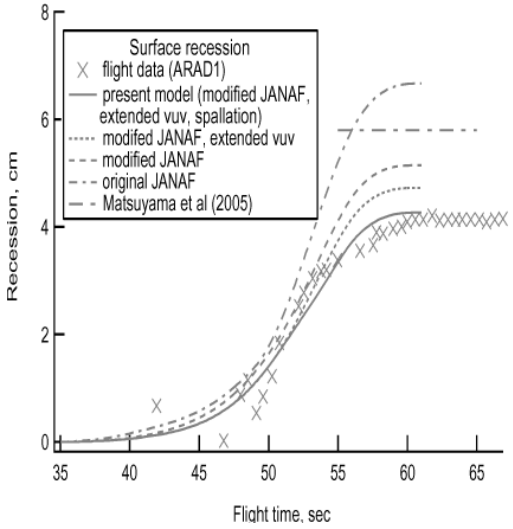

Figure 25. Comparison between the observed surface recession and calcul-altion[22] at the stagnation point of Galileo Probe.

For the Galileo Probe, at the stagnation point and at the peak-heating point in the flight trajectory, Park calculated that the radiative heat flux at the boundary layer edge was 34.5 kW/cm^2. After absorption by boundary layer and blocking by solid particles, the radiative flux that reached the wall was 14.7 kW/cm^2. In comparison, the convective heat flux was 0.14 kW/cm^2. The portion of radiative heat flux that did not reach the wall, 34.5 - 14.7 = 19.8 kW/cm^2, was convected downstream.

The extent of radiation absorption in the boundary layer calculated by Park was larger than those calculated by others. The large absorption resulted in Park's calculation because more abosorption bands were accounted for. Here we see the need for more thorough accounting of absorption mechanisms in the boundary layer, as well as the effect of solid particles.

3.1.3. Stardust

In Fig. 26, similar plot is shown for the Stardust entry vehicle.[23] At the peak-heating point, at the boundary layer edge, radiative heat flux was calculated to be 913 W/cm^2. Of this, 484 W/cm^2 was converted into convective heat flux to make the resulting convective heat flux to be 967 W/cm^2. In the absence of radiation, convective heat flux would have been 483 W/cm^2. That is, about half of convective heat flux was due to radiation absorption. The radiative heat flux reaching wall was only 129 W/cm^2.

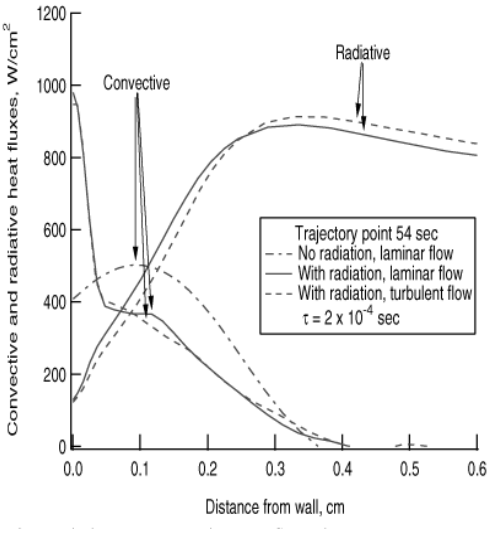

Figure 26. Distribution of radiative heat flux along stagnation streamline at peak-heating point of Stardust entry.[23]

3.2. Radiative to Convective Heat Flux Conversion

The above three cases show that half or more of radiative heat flux present at the edge of boundary layer is converted to convective heat flux. This conversion occurs as a result of absorption of the vacuum ultra-violet component of radiation. In the past, there was a erroneous understanding that the radiation absorbed in the boundary layer is heat flux vanished, and therefore needs not be concerned. That reasoning led one to believe that the vacuum ultra-violet component of radiation needs not be included in calculating the heat transfer rates. The above examples show that that approach is wrong.

One wonders what exactly happens to the radiative heat flux incident on the boundary layer edge. For that purpose, we draw control volumes as shown in Fig. 27. Using a drastically simplified flow model, one can calculate how the heat fluxes are distributed. Without going into the details, one can say that all absorbed radiative heat flux manifests itself as convective heat flux. But the distribution of this increment in convective heat flux will depend on where in the boundary layer the absorption occurs. If absorption occurs near the wall, the absorbed radiative energy shows up as convective energy immediately downstream. If absorption occurs near the boundary layer edge, the increment in convective heat flux will occur over a wide range downstream.

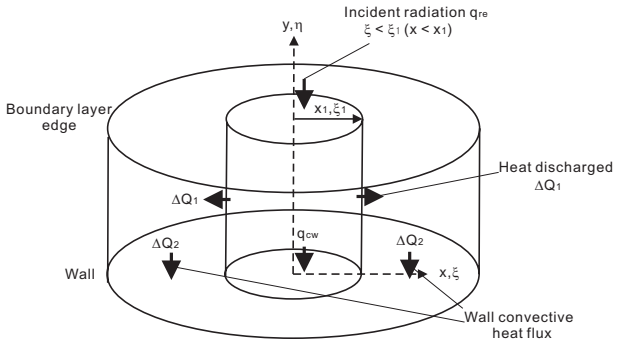

Figure 27. Control volumes in considering radiation-to-convection flux conversion.

Where in the boundary layer absorption will occur depends on the chemical state of the boundary layer flow. This point needs careful study in the future.

3.3. Radiation Intensity Calculation

Radiation calculation is made in the aerothermodynamics community using computer codes that descended from the NEQAIR85 package. The latest of this class of codes is SPRADIAN07 developed jointly by Japan Aerospace Exploration Agency (JAXA) and Korea Advanced Institute of Science and Technology (KAIST).[24] The calculation method is still incomplete, as follows:

3.3.1. Pseudo Continua of Atomic Radiation

Atomic radiation is calculated line-by-line using the data in the NIST data base.[25] But the NIST data base does not contain the pseudo continua. Pseudo continua are line radiations emanating from very high principal quantum number states. For these lines, wavelength is uncertain and linewidth is very large, i.e. up to 1000 nm or more. They are individually very weak, but there are so many of them. As a result, they look like a continuum. The intensity parameters for these lines are known from the Opacity Project.[26] Someone will have to take time to put them into the radiation code.

3.3.2. Symmetries in Diatomic Molecules

The existing radiation codes do not account for all possible symmetries. SPRADIAN07 has the most, but is still incomplete.

3.3.3. More Diatomic Systems

As the case of Galileo Probe shows, the diatomic data base is still far from complete in the vacuum ultra-violet wavelength range. As mentioned, these vacuum ultra-violet bands

have been neglected in the past because of ignorance. Now that we know, we should put all of them into the data base.

In this connection, it should be emphasized that we aerospace engineers can no longer count on physicists or chemists to carry out such calculations. Computer codes to calculate diatomics using quantum mechanics are already available commercially. Engineers should acquire these codes and calculate radiation by themselves.

3.4. Effect of Solid Particles

An ablating heatshield produces solid particles. There are two mechanisms by which solid particles are produced: ejection by internal pressure of pyrolysis and by shear force. The modern computer code describing material response describes the internal pressures.[27] Experiments to measure the internal pressures are in progress.[28] This is a temperature-driven phenomenon, and occurs when surface temperature becomes high. In contrast, particle production by shear force is a pressure-driven phenomenon and occurs when pressure is high. There has been many experimental evidences showing the presence of solid particles.[22]

Park et al[29] made a systematic study of the solid particles in an arc-jet wind tunnel. During the entry flight of the Stardust vehicle, radiation from the shock layer was observed from an airborne platform.[30] The measured spectrum showed strong CN radiation. Such strong CN radiation can occur only if carbon is present in the inviscid region of the shock layer in a concentration larger than can be accounted for by the atmospheric CO_2. Such large concentration of carbon species in the inviscid region of the shock layer can occur only if solid carbon particles are ejected from the ablating wall.

Park et al[29] reasoned that solid particles can radiate as a black body, and simultaneously block radiation produced by hot gases. Depending on the condition, one effect may be stronger than the other. One wonders also what effects the solid particles will bring to the turbulence level.

By analyzing several experimental clues, Park[31] reasoned that ablation produces turbulence. The injection-induced turbulence model was able to explain the large ablation in the downstream region of the Galileo Probe heat shield.[21] Ablation accompanies both injection of the pyrolysis gas from the pores on the surface and injection of solid particles. Which of these two phenomena produces turbulence is not known. These remain to be studied in the future.

4. Conclusion

In the above, we have identified the following topics to be studied in the future:

1. Molecular dynamics calculations for state-to-state collisional transition rate determination including vibrational and rotational states.

2. Handling large number of state-to-state transitions in integrating the master equation.

3. Determining the so-called collision-limiting cross sections in two-temperature model and diffusion correction paramters.

4. Deriving a three-temperature model accounting for slow rotational relaxation at high temperatures.

5. Developing piston compression-driven shock tubes to produce 12 km/s shock speed in air, CO_2, SO_2, and H_2O and 30 km/s shock speed in H_2 + He mixtures.

6. Shock tube experiments for gases of atmospheres of Jupiter's and Saturn's moons.

7. Quantum-mechanical calculations of radiation intensity parameters for diatomics, especially for the vacuum ultra-violet wavelength range.

8. Development of the model describing radiation-controlled reaction rates for ionization of hydrogen.

9. Modeling of coking process in heatshields.

10. Modeling of radiation-to-convection conversion processes.

11. Investigation of effects of particles produced by ablation.

12. Investigation of turbulence produced by ablation.

References

1. Park, C., "Blocking Sun with Orbiting Balloons," Proceedings of the Global Conference on Global Warming 2008 (GCGW-08) 6-10 July 2008, Istanbul, Turkey, paper No. 359.

2.Nompelis, I., Candler,G. V., and Holden, M. S., "Effect of Vibrational Nonequilibriuim on Hypersonic Double-Cone Experiments," AIAA Journal, Vol. 41, No. 11 (2003) pp. 2162-2169.

3. Nonaka, S., and Takayama, K., "Ballistic Range Measurement of the Shock Shapes in Intermediate Hypersonic Regime," AIAA Paper 99-1025 (1999).

4. Furudate, M., and Sawada, K., "Effect of Rotational Nonequilibrium on Shock Stand-off Distance in Intermediate Hypersonic Range," AIAA Paper 2001-0813 (2001)

5. Park, C., "Nonequilibrium Air Radiation (NEQAIR) Program: User's Manual," NASA TM 86707, July 1985.

6. Sharma, S. P., and Gillespie, W., "Nonequililbrium and Equilibrium Shock Front Radiation Measurements," Journal of Thermophysics and Heat Transfer, Vol. 5, No. 3, (1991) pp. 257-265.

7. Fujita, K., Sato, S., Abe, T., and Ebinuma, Y., "Experimental Investigation of Air Radiation Behind a Strong Shock Wave," AIAA Paper 98-2467 (1998)

8. Koreeda, J., "An Expermental Study on Nonequilibrium Radiation of Strong Shock Waves in Air," Ph.D Thesis, Chiba University, Chiba, Japan, January 1995.

9. Miyazaki, K., Ando, H.,Takeda, K., Toyoda, K, and Maeno, K., "Establishment of Coherent Anti-Stokes Raman Spectroscopy Measurement System for Radiative Flow Behind Hyperveolocity Shock Waves," paper presented at 25th International Symposium on Shock Waves, Bangalore, India, July 2004.

10. Park, C., "Rotational Relaxation of N_2 Behind a Strong Shock Wave," Journal of Thermophysics and Heat Transfer, Vol. 18, No. 4, (2004) pp. 527-533.

11. Sharma, S. P., and Schwenke, D. W., "The Rate Parameters for Coupled Rotation-Vibration Phenomenon in H2," Journal of Thermophysics and Heat Transfer, Vol. 5, No. 4, (1991) pp. 469-480.

12. Furudate, M., Fujita, K., and Abe, T., "Coupled Rotational-Vibrational Relaxation of Molecular Hydrogen at High Temperatures," Journal of Thermophysics and Heat Transfer, Vol. 20, No. 3, (2006) pp. 457-464.

13. Kim, J. G., Kwon, O. J., and Park, C., "State-to-State Rate Coefficients and Master Equation Study for H2 + H and + He," AIAA Paper 2008-1265 (2008)

14. Park, C., "Thermochemical Relaxation in Shock Tunnels," Journal of Thermophysics and Heat Transfer, Vol 20, No. 4, (2006) pp. 689-698.

15. Furudate, M., Jeung, I-S., and Matsuyama, S., "Nonequilibrium Calculation of Flowfield Over Galileo," AIAA Paper 2006-0383 (2006).

16. Leibowitz, L. P., "Measurement of the Structure of Ionizing Shock Wave in a Hydrogen-Helium Mixture," The Physics of Fluids, Vol. 16, No. 1 (1973) pp. 59-68

17. Bogdanoff, D. W., and Park, C., "Radiative Interaction Between Driver and Driven Gases in an Arc-Driven Shock Tube," The Journal of Shock Waves, Vol. 12, No. 3 (2002) pp. 205-214.

18. Park, C., "Effect of Lymann Radiation on Nonequilibrium Ionization of Atomic Hydrogen," AIAA Paper 2004-2277 (2004).

19. Morgan, R. G., McIntire, T. J., Buttsworth, D. R., Jacobs, P. A., Potter, D. F., Brandis, A. M., Gollan, R. J., Jacobs, C. M., Capra, B. R., McGilvray, M., and Eichmann, T., "Impulse Facilities for the Simulation of Hypersonic Radiating Flows," AIAA Paper 2008-4270 (2008).

20. Park, C., "Stagnation-Point Radiation for Apollo 4," Journal of Thermophysics and Heat Transfer, Vol. 18, No. 3 (2004) pp 349-357

21. Matsuyama, S., Ohnishi, N., Sasoh, A., and Sawada, K., "Numerical Simulation of Galileo Probe Entry Flowfield with Radiation and Ablation," Journal of Thermophysics and Heat Transfer, Vol. 19, No. 1 (2005) pp. 28-35

22. Park, C., "Stagnation Region Heating Environment of Galileo Probe," AIAA Paper 2008-4109 (2008)

23. Park, C., "Calculation of Stagnation-Point Heating Rates Associated with Stardust Vehicle," Journal of Spacecraft and Rockets, Vol. 44, No. 1 (2007) pp. 24-32 .

24. Hyun, S. Y., Park, C., and Chang, K. S., "Rate Parameters for Electronic Excitation of Diatomic Molecules, III. CN Radiation Behind a Shock Wave," AIAA Paper 2008-1276 (2008)

25. http://physics.nist.gov/PhysRefData/ASD/index.html

26. http://vizier.u-strasbg.fr/topbase.html

27. Ahn, H. K., Park, C., and Sawada, K., "Response of Heatshield Material at Stagnation Point of Pioneer-Venus Probes," Journal of Thermophysics and Heat Transfer, Vol. 16, No. 3, (2002) pp. 432-439.

28. Suzuki, T., Sawada, K., Yamada, T., and Inatani, Y., "Experimental and Numerical Study of Pyrolysis Gas Pressure in Ablating Test Piece," Journal of Thermophysics and Heat Transfer, Vol. 19, No. 3 (2005) pp. 266-272.

29. Park, C., Raiche, G. A., II, and Driver, D. M., "Radiation of Spalled Particles in Shock Layers," Journal of Thermophysics and Heat Transfer, Vol. 18, No. 4, pp 519-526 (2004)

30. Winter, M., and Herdrich, G., "Heat Shield Temperatures and Plasma Radiation Obtained From Spectroscopic Observation of the Stardust Reentry in the Near UV," AIAA Paper 2008-1212 (2008)

31. Park, C., "Injection-Induced Turbulence in Stagnation-Point Boundary Layers," AIAA Journal, Vol. 22, No. 2, pp.. 219-225 (1984)